Semnan University

Mechanics of Advanced Composite Structures

journal homepage: http://MACS.journals.semnan.ac.ir

An Investigation on Three-Point Bending of Foam-Filled Double Tubes and Parameter Optimization Using Response Surface Methodology

A. Kami [a,*], J. Shahbazi Karami [b]

[a] *Faculty of Mechanical Engineering, Semnan University, Semnan, 3513119111, Iran*
[b] *Faculty of Mechanical Engineering, Shahid Rajaee Teacher Training University, Tehran, 1678815811, Iran*

KEYWORDS

Foam-filled tubes
Composite foam
Design of experiments
Response surface methodology (RSM)
Optimization

ABSTRACT

The bending behavior of foam-filled double (FFD) tubes was studied in this study. The goal was to create an optimal structure that could absorb the most energy while weighing the least. On aluminum FFD tubes composed of inner and outer tubes (1100 aluminum alloy) and a composite foam core (with A356 cast alloy base and 0.6 g/cm^3 density), three-point bending tests were conducted. Additionally, a finite element model of tube bending was developed and its outputs were validated using experimental data. Following that, the response surface methodology (RSM) was used to (numerically) investigate the influence of inner and outer tube diameters, inner and outer tube thickness, and foam density on bending energy and weight of FFD tubes. The impact of the investigated factors was investigated using analysis of variance (ANOVA). Finally, RSM was used to compute the best values of the parameters that result in the maximum energy absorption in bending and the lightest weight of the FFD tube. The optimization process resulted in a 141.4% increase in absorbed bending energy and a 4.63% reduction in the FFD composite tube's weight (in comparison to the initial design of the FFD tube).

1. Introduction

The application of foam-filled tubes in the automotive and aerospace industries has been received more attraction in the last few years [1]. This is because foam-filled tubes have higher energy absorption capability in comparison with empty tubes. In recent researches, different forms of foam-filled tubes have been inspected such as a foam-filled (single) tube, FFD tubes, tubes filled with functionally graded foams, partially filled tubes, and so on [2-4].

Different configurations of the foam-filled tubular structures have been tested in different loading conditions. In the case of bend loading, the effect of parameters such as foam type and density, tube shape, adhesion between the foam and tube, and so on have been examined. Santosa et al. [5, 6] conducted numerical and experimental studies on the bending behavior of empty and foam-filled square tubes and showed that filling the tube with foam, significantly increases the bending strength of the tubes. Kim et al. [7] filled cylindrical tubes with piecewise foams with various densities and conducted experimental and numerical tests of three-point bending. They concluded that the bending resistance of a tube with 3 pieces of foam is higher than tubes with 1 and 4 pieces of the filler foam. Hanssen et al. [8] numerically simulated axial compression and three-point bending of circular and square foam-filled tubes. They analyzed the effect of the foam density on the deformation behavior of the tubes. Guo et al. [9, 10] performed quasi-static three-point bending tests on empty, foam-filled single and double tubes and studied the effects of filler foam arrangements on the behavior of the tube. They found that the FFD tube has a much higher maximum displacement and more energy absorption capacity before failure in comparison with the empty and foam-filled single tubes. Shojaeifard et al. [11] numerically investigated the energy absorption behavior of empty and foam-filled tubes with circular, square, and elliptic cross-sections. It was found that the

* Corresponding author. Tel.: +98-23-31532353
E-mail address: akami@semnan.ac.ir

DOI: 10.22075/MACS.2021.20410.1259
Received 2020-05-14; Received in revised form 2021-02-17; Accepted 2021-04-01

elliptic foam-filled aluminum tube has much greater specific energy absorption than that of the circular and square tubes. Duarte et al. [12] assessed the deformation of in-situ foam-filled tubes in quasi-static and dynamic bending loadings. They analyzed the effect of manufacturing parameters such as the structural changes in the thermally treated tubes, the surface roughness derived from oxidation, and the dimensions of the interface gap between the foam and tube on the bending performance of the in-situ foam-filled tubes. The results obtained by Duarte et al. [12] suggest that in-situ manufacturing of foam-filled tubes will provide a stable and controllable deformation along with a promising energy absorption capability. Vesenjak et al. [13] conducted quasi-static and dynamic three-point bending tests on the tubes filled with advanced pore morphology (APM) foam, hybrid APM foam, metallic hollow sphere structures (MHSS), and ex-situ and in-situ closed-cell aluminum alloy foams. Their results showed that the hybrid APM and the ex-situ foam-filled tubes have the highest peak in the bending load curve along with a rapid load drop and abrupt failure at the onset of the peak load. On the other hand, APM, MHSS and in-situ foam filled tubes showed a more ductile behavior in comparison with the other types of tubes.

The above literature survey reveals part of efforts made for achieving foam-filled structures with high energy absorption capacity and reliable bending behavior. Despite this, yet a vast scope of research exists for optimizing the foam-filled tubes for a variety of applications. Hence, this research is carried out (a) to study the effects of the inner and outer tubes' diameter and thickness, and the foam density on the absorbed bending energy, (b) to derive a simple yet accurate equation for the prediction of the bending energy of the FFD tubes, and (c) to optimize the FFD tube's structure.

2. Experiments

The FFD tube has been made of AA1100 inner and outer tubes and A356 foam as the (filler) core. The inner and outer tubes' diameters and thickness are 21.5 mm, 39.6 mm, 0.75 mm, and 1.65 mm, respectively. The foam is made in the form of a thick plate and is machined to a tubular shape. As shown in Fig. 1 (a), the components of the FFD tube are adhesively bonded to each other. In Fig. 1 (b), a sample of the FFD tube and its components are illustrated.

The foam is fabricated by the stir casting process and using A356 cast aluminum alloy as the base material, SiC particles with 98.0 wt.% purity and 10 μm mean mass particle size as the reinforcement phase and $CaCO_3$ powder with 99.5 wt.% purity and 5 μm average size as the blowing agent [14]. Both reinforcement and blowing agent are preheated to improve their wettability and to remove the adsorbed gases. The final cast composite foam has 3 wt.% SiC and 5 wt.% $CaCO_3$ and its porosity and density are equal to 86% and 0.6 g/cm^3, respectively. A scanning electron microscope (SEM) image of the composite foam is depicted in Fig. 2.

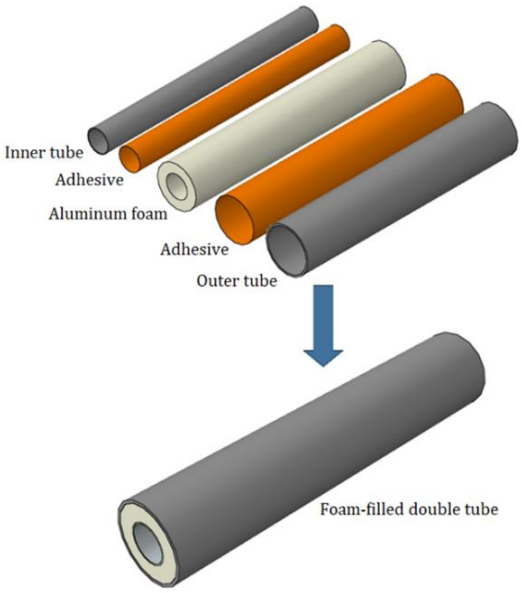

(a)

(b)

Fig. 1. (a) structural components of the FFD tube and (b) a sample of the FFD tube and its components

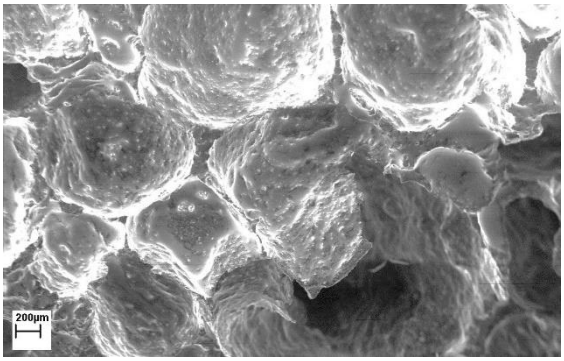

Fig. 2. SEM of the A356 composite foam with 86% porosity and 0.6 g/cm^3 density [14]

The gluing surfaces of the outer and inner tubes were abraded using different sandpapers and then cleaned with acetone. The tubes and foam were glued using Akfix 610 polyurethane-based adhesive.

The compressive properties of the composite foam are determined by conducting compression tests according to DIN 50134:2008 standard [15]. The tests are performed on cuboid samples with 30 mm × 30 mm × 40 mm dimensions and with a speed of 0.5 mm/min. The mechanical properties of the foam are reported in Table 1. Furthermore, the mechanical properties of the inner and outer tubes are derived from tensile tests (according to ASTM E8M [16]), which are listed in Table 1. The strength coefficient, K, and strain-hardening exponent, n, are the parameters of Hollomon's equation ($\sigma = K\varepsilon^n$), which are derived by interpolating the true stress-true strain curve.

Three-point bending tests are conducted on the composite foam for further exploration of its mechanical properties, which resulted in bending strength of 3.8 MPa at an elongation of about 1%. Moreover, Three-point bending tests are conducted on the inner, outer, and FFD tubes. As shown in Fig. 3, the total length of the tubes and the supports distance are equal to 200 mm and 160 mm, respectively. Bending tests are performed with the punch travel speed of 6 mm/min using a Santam® hydraulic press with a maximum capacity of 40 tons.

3. Finite Element Modeling and Design of Experiments

3.1. FE Modeling of Three-point Bending

The FE model of the three-point test is established in the commercial Abaqus software. The FE analysis was performed using the Abaqus/explicit quasi-static solver. In this model, the inner and outer tubes, and the foam core are defined as deformable, while the supports and the punch are set as rigid. The mechanical properties of the deformable components are specified according to Table 1. Hollomon's hardening law with Mises yield function was used to model the plastic deformation of the materials [17, 18]. By considering the symmetry of the bending test setup, just one-quarter of the deformable components are modeled (see Fig. 4). The C3D8R element with the size of 1 mm (with 2 elements through-thickness) is used to mesh the deformable components, which results in the total number of 46200 elements in the FE model.

The contact between the punch and tube and also between the supports and tube is defined by the Coulomb friction law with a friction coefficient of 0.15. Because there was no slide between the foam and the tubes, the foam is tied to the inner and outer tubes.

Table 1. Mechanical properties of the AA1100 tubes and the composite foam

Property	AA1100	Composite foam [14]
Young modulus (GPa)	70	0.3
Poisson's ratio	0.30	0.01
Density (g/cm^3)	2.78	0.60
Yield strength (MPa)	92.1	7.3
Strength coefficient, K (MPa)	230	-
Strain-hardening Exponent, n	0.169	-

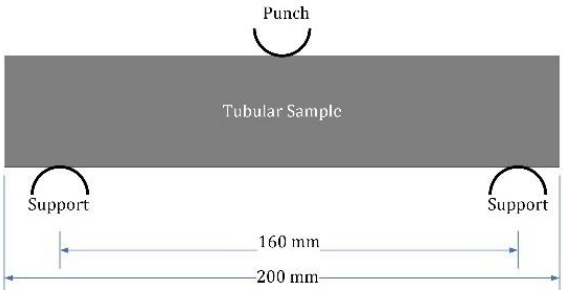

Fig. 3. Schematic of three-point bending test on tubes with the total length of 200 mm

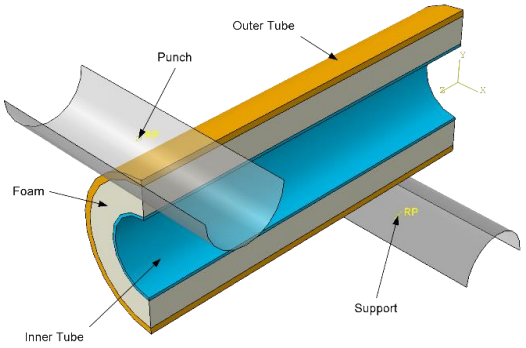

Fig. 4. Three-dimensional representation of the three-point bending test components in the FE model

3.2. Design of Experiments

To study the effect of parameters including the inner and outer tubes' diameters, inner and outer tubes' thickness and foam density on the bending energy and FFD tube weight, RSM design of experiments (DOE) are deployed. The Design-Expert® V9 software is used to design the experiments. Consequently, a reasonable number of experiments are designed and also it becomes possible to perform ANOVA and optimization of parameters with a fair effort [19].

In the designed experiments, the outer tube's diameter value (D_o) must be larger than the inner tube's diameter (D_i). To ensure the fulfillment of this constraint, D_o is replaced by a new parameter (D_o - D_i) > 0, which guarantees that D_o will always be larger than D_i. The parameters D_i, (D_o - D_i), the thicknesses (t_i, t_o) and the foam density, ρ_{foam} are set to (10 – 30) mm, (10 – 50) mm, (0.5 – 2)

mm and (0.4 – 0.7) g/cm^3 ranges, respectively. The geometric parameters are illustrated in Fig. 5. The experiments are generated by the face-centered central composite design, which results in 43 experiments. These experiments are presented in Table 2. Because, carrying out 43 experimental bending tests is very expensive and time-consuming, the designed experiments are numerically simulated using the developed FE model.

To have a light FFD tube with high energy absorption capability, two design outputs including the tube weight and the bending energy are considered. The value of the bending energy for each design is obtained by calculating the area under the force-displacement curve. Furthermore, Eq. (1) is used to determine the FFD tubes weight:

$$M = \frac{\pi L}{4}\begin{Bmatrix}\begin{bmatrix} D_i^2 - (D_i - 2t_i)^2 + D_o^2 \\ -(D_o - 2t_o)^2 \end{bmatrix}\rho_{Al} \\ +[(D_o - 2t_o)^2 - D_i^2]\rho_{foam}\end{Bmatrix} \quad (1)$$

where, $\rho_{Al} = 2.78$ g/cm^3 and $L = 200$ mm are the density and length of the tubes, respectively.

4. Results and Discussions

4.1. Experimental Three-point Bending Tests

Deformation of inner and outer tubes and FFD tube during the three-point bending test is illustrated in Figs. 6-8. Furthermore, the longitudinal section of the FFD tube is illustrated in Fig. 9.

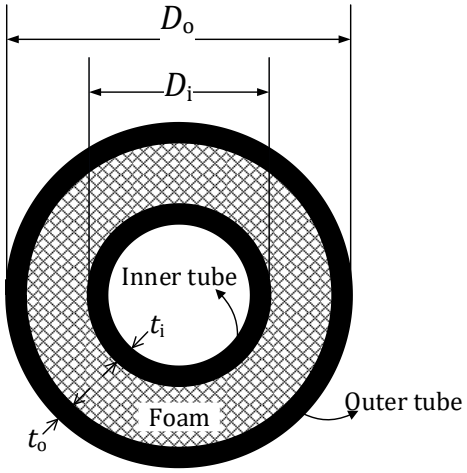

Fig. 5. The schematic illustration of the geometric parameters of FFD tube

Table 2. Designed experiments for FE simulations of three-point bending tests of the FFD tube and their outputs

Test No.	D_i (mm)	$D_o - D_i$ (mm)	t_i (mm)	t_o (mm)	ρ_{foam} ($\frac{g}{cm^3}$)	M (g)	F_{max} (N)	E (kJ)
1	30	10	0.50	0.50	0.70	128.54	4.78	136.13
2	10	30	1.25	1.25	0.55	216.56	10.69	277.97
3	30	30	1.25	1.25	0.55	398.93	19.26	459.35
4	10	50	2.00	2.00	0.40	421.33	23.20	531.51
5	30	50	2.00	0.50	0.7	754.52	43.74	234.07
6	10	10	0.50	2.00	0.40	80.98	2.43	77.16
7	30	10	0.50	2.00	0.70	202.06	8.42	250.85
8	10	10	2.00	0.50	0.40	61.38	2.02	62.09
9	20	30	1.25	1.25	0.40	264.01	11.26	289.52
10	30	10	2.00	0.50	0.40	171.33	6.23	185.81
11	20	30	1.25	2.00	0.55	356.88	18.88	483.92
12	30	50	0.50	0.50	0.40	430.78	15.00	338.73
.	.	.	.	.	.	.	.	.
.	.	.	.	.	.	.	.	.
.	.	.	.	.	.	.	.	.
32	10	50	0.50	2.00	0.40	401.67	20.66	481.71
33	10	50	0.50	0.50	0.40	272.70	10.65	256.39
34	10	50	0.50	0.50	0.70	432.02	10.65	256.39
35	30	10	2.00	0.50	0.70	200.60	8.22	245.15
36	30	50	2.00	2.00	0.40	676.67	28.83	634.83
37	10	10	2.00	2.00	0.70	107.98	3.91	124.13
38	20	30	1.25	1.25	0.55	307.75	15.27	383.07
39	10	10	0.50	0.50	0.40	41.73	0.91	28.74
40	30	50	2.00	0.50	0.40	502.83	19.46	427.06
41	20	30	0.50	1.25	0.55	283.84	13.84	343.12
42	10	10	2.00	0.50	0.70	73.68	2.18	67.89
43	20	30	1.25	0.50	0.55	257.04	11.31	276.92

Fig. 6. Deformation of the inner tube during three-point bending test

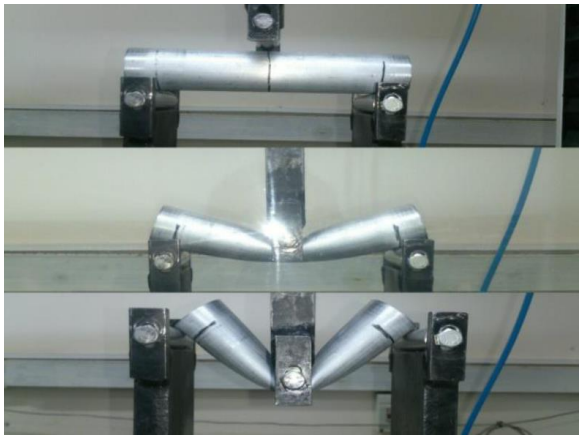

Fig. 7. Deformation of the outer tube during three-point bending test

Fig. 8. Deformation of the FFD tube during three-pint bending test (from start to fracture)

Fig. 9. The longitudinal section of the bent FFD tube

The bending force-displacement curves of the bending tests are depicted in Fig. 10. The results indicate that the inner tube has a very low flexural resistance, where its maximum bending force and energy are about 0.43 kN and 10.7 kJ, respectively. The outer tube has more rigidity and its maximum bending force and energy are about 3.72 kN and 103.6 kJ, respectively. On the other hand, the FFD tube's maximum bending force and energy are 10.1 kN and 280.9 kJ, respectively, which are much higher than the values observed in the bending of the inner and outer tubes. This observation has resulted from the use of a foam layer between the inner and outer tubes.

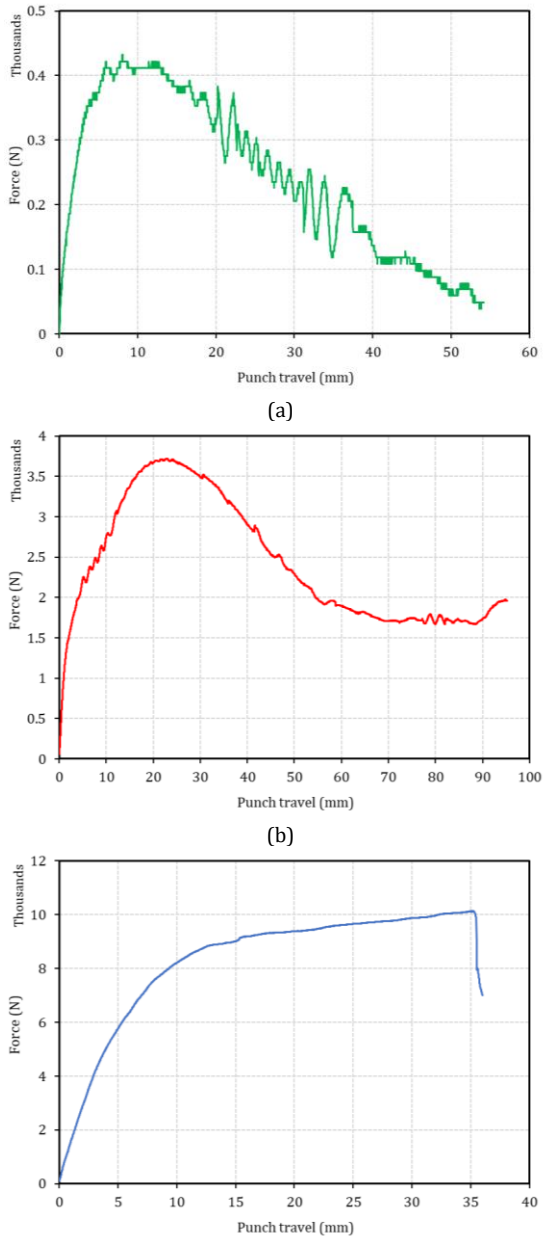

Fig. 10. Force-displacement curve of (a) inner tube, (b) outer tube, and (c) FFD tube in three-point bending with the tube length of 200 mm

4.2. Validation of the FE Model

The FE model of the three-point test is validated by comparing its results with the results of the experimental tests. Comparison of the FFD tube deformed shapes (experimental and FE simulation) at the punch travel of 35 mm is shown in Fig. 11. As this figure depicts, the FE simulation provides a good prediction of the experimental test, qualitatively. A more sustainable comparison is presented in Fig. 12, which shows the force-displacement curves of the FE simulation and the experimental test. The maximum deviation of the FE curve from the experimental curve is about 10%, which indicates the good accuracy of the FE model. It is worth mentioning that, the relative error in the prediction of the maximum bending force is about 0.57% (maximum bending force: experimental test = 10.12 kN, FE simulation = 10.07 kN). From Fig. 12, one may notice that the FE force-displacement curve is extended beyond the fracture point, which is because the FE model doesn't take into account any damage or fracture in the deformable components.

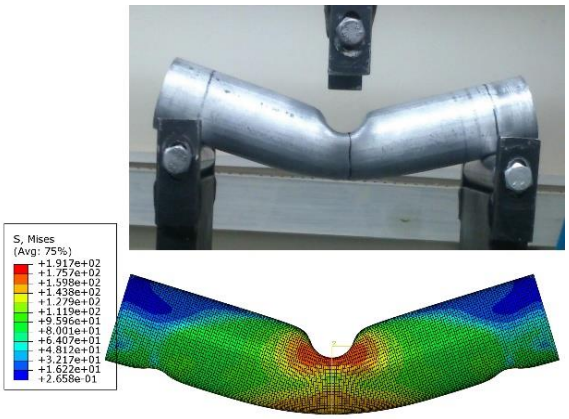

Fig. 11. Comparison of FE simulation and experimental test results at the fracture point

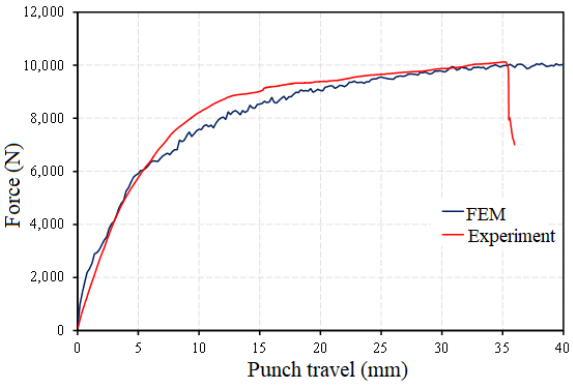

Fig. 12. Comparison of FE force-displacement curve with the experimental test curve in three-point bending of FFD tube

4.3. Analysis of Variance (ANOVA)

After validation of the FE model, it was used for the calculation of the bending force and energy. Using FE simulations, the bending force-displacement diagram and the absorbed energy of each design (each row of Table 2) were obtained. Furthermore, the FFD tube weight for each design was calculated using Eq. (1). The values of the FFD tubes' bending energy and weight (along with the maximum bending force) are summarized in Table 2.

The effectiveness of each studied parameter is determined by performing ANOVA on the data given in Table 2. The results of the ANOVA are listed in Table 3. According to this table, almost all parameters are important in the estimation of bending energy and weight of FFD tube (see p-values in Table 3). On the other hand, D_o-D_i has the highest effect on both bending energy and weight and ρ_{foam} and t_i have the least effect on the bending energy and weight, respectively (see F-vales in Table 3).

Table 3. A summary of the ANOVA results regarding the effect of the studied parameters on the FFD tube bending energy and weight

Parameter	Sum of squares	Mean of squares	F-value	p-value
Bending energy function	0.048	2.419E-003	31.65	< 0.0001
D_i	6.352E-003	6.352E-003	83.10	< 0.0001
D_o-D_i	0.024	0.024	307.48	< 0.0001
t_i	1.677E-003	1.677E-003	21.94	0.0001
t_o	5.382E-003	5.382E-003	70.41	< 0.0001
ρ_{foam}	8.833E-004	8.833E-004	11.56	0.0026
Residual	1.682E-003	7.643E-005		
Weight function	26.46	1.32	1173.56	< 0.0001
D_i	3.98	3.98	3531.16	< 0.0001
D_o-D_i	19.22	19.22	17052.62	< 0.0001
t_i	0.37	0.37	326.73	< 0.0001
t_o	1.19	1.19	1057.01	< 0.0001
ρ_{foam}	0.58	0.58	514.47	< 0.0001
Residual	0.025	1.127E-003		

Data presented in Table 2 make it possible to find a quadratic function for both tube's bending energy (Eq. (2)) and weight (Eq.(3)).

$$\begin{aligned}1/\sqrt{E} = {} & 0.367006 - 0.185304 \times \rho_{foam} - 0.057378 \times t_o \\ & - 0.052565 \times t_i - 0.005424 \times (D_o - D_i) \\ & - 0.005701 \times D_i + 0.004496 \times \rho_{foam} \times t_o \\ & + 0.019183 \times \rho_{foam} \times t_i \\ & + 0.000299 \times \rho_{foam} \times (D_o - D_i) \\ & + 0.000100 \times \rho_{foam} \times D_i + 0.004764 \times t_o \times t_i \\ & + 0.000316 \times t_o \times (D_o - D_i) + 0.000462 \times t_o \times D_i \\ & + 0.000447 \times t_i \times (D_o - D_i) + 0.000393 \times t_i \times D_i \\ & + 0.000059 \times D_i(D_o - D_i) + 0.100687 \times \rho_{foam}\text{^}2 \\ & + 0.005383 \times {t_o}^2 + 0.002172 \times {t_i}^2 \\ & + 0.000030 \times (D_o - D_i)^2 + 0.000036 \times {D_i}^2 \end{aligned} \quad (2)$$

$$\begin{aligned}M = {} & 127.696 - 232.241 \times \rho_{foam} + 16.407600 \times t_o \\ & + 0.001103 \times t_i - 8.20742 \times (D_o - D_i) \\ & - 4.75116 \times D_i - 29.8444 \times \rho_{foam} \times t_o \\ & + 14.9225 \times \rho_{foam} \times (D_o - D_i) \\ & + 8.64 \times \rho_{foam} \times D_i + 1.40117 \times t_o \times (D_o - D_i) \\ & + 1.40133 \times t_o \times D_i + 1.74667 \times t_i \times D_i \\ & + 0.172788 \times (D_o - D_i) \times D_i + 0.107926 \times {\rho_{foam}}^2 \\ & - 1.40013 \times {t_o}^2 - 1.74679 \times {t_i}^2 \\ & + 0.086394 \times (D_o - D_i)^2 - 0.000026 \times {D_i}^2 \end{aligned} \quad (3)$$

Equations (2) and (3) are used as the fitness functions in the multi-objective optimization of three-point bending of the FFD tube (see section 4.4). Referring to Table 3, these two fitness functions have a low (mean/sum) of squares of errors, which certifies their ability in the good prediction of their related functions. This could be better observed from Fig. 14, which shows the predicted values (of the quadratic function of energy) against the real value (obtained from the FE simulations of the bending test). As this figure depicts, the predicted values are very close to the real values (or bisector line). In this case, the adjusted R-squared value is equal to 0.936. Almost the same results are obtained for the quadratic function of FFD tube weight.

The perturbation plots of the FFD tube's bending energy and weight are shown in Fig. 13. These plots depict the change of the FFD tube's bending energy and weight in the central point in the design space (-1, and +1 indicate the upper and lower limits of the design space). According to the perturbation plot in Fig. 13(a), the parameters with the highest and the lowest effect on the FFD tube's bending energy are (D_o - D_i) and ρ_{foam}, respectively. For the weight of the FFD tube, (D_o - D_i) is the most affecting parameter, while t_i has the least effect (Fig. 13(b)).

Response surface plots are useful tools to show the effect of studied parameters on the outputs. Two examples of them are shown in Fig. 15, which illustrate the effect of the inner and outer tubes' thickness on the bending energy (Fig. 15(a)) and the inner tube's diameter and foam density on the bending energy (Fig. 15(b)). According to Fig. 15(a), the highest bending energy will be achieved when the inner and outer tubes' thicknesses have the highest value (2 mm for both thicknesses). Furthermore, Fig. 15(a) shows that no interaction exists between the inner and outer tubes' thickness. Similarly, the highest bending energy is belonging to an FFD tube with the highest inner tube's diameter (30 mm) and the highest foam density i.e. 0.7 g/cm^3 (Fig. 15(b)). From Fig. 14(b), one may notice that the bending energy has a curved response surface. It means that the foam density and the inner tube's diameter have an interacting effect on the bending energy. The interacting parameters have been included in Eqs. (2) and (3). The higher the coefficient of a (bivariate) term, the higher the interaction between its variable (parameters). Analogous surface plots could be drawn for other combinations of parameters and also for the weight function.

4.4. Optimization of the Parameters

Multi-objective optimization to find an FFD tube design with the lowest weight and highest energy absorption capability is done using Design-Expert® V9 software. The quadratic functions of the FFD tube weight and bending energy are used as the fitness functions. Furthermore, the studied parameters (D_i, D_o – D_i, t_i, t_o and ρ_{foam}) are constrained to change in the same range used in the DOE (see Table 2).

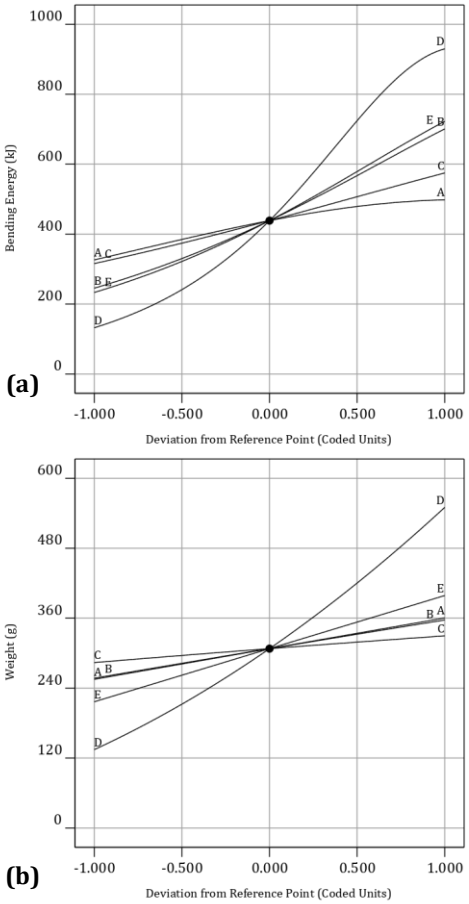

Fig. 13. Perturbation plot of the FFD tube's (a) bending energy, and (b) weight; *A*, *B*, *C*, *D*, *E*, are ρ_{foam}, t_o, t_i, D_o-D_i, and D_i, respectively

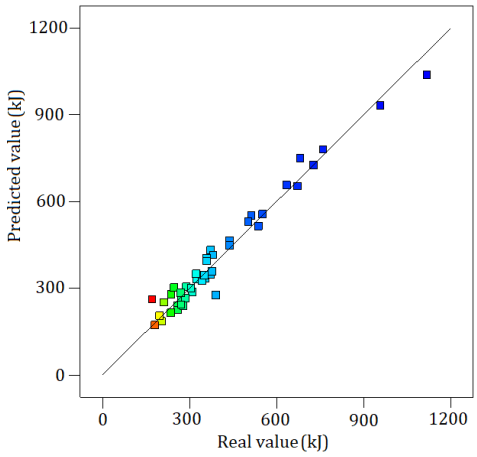

Fig. 14. The predicted value of bending energy (by the energy quadratic function) concerning the real values of the bending energy (obtained from FE simulations, see Table 2)

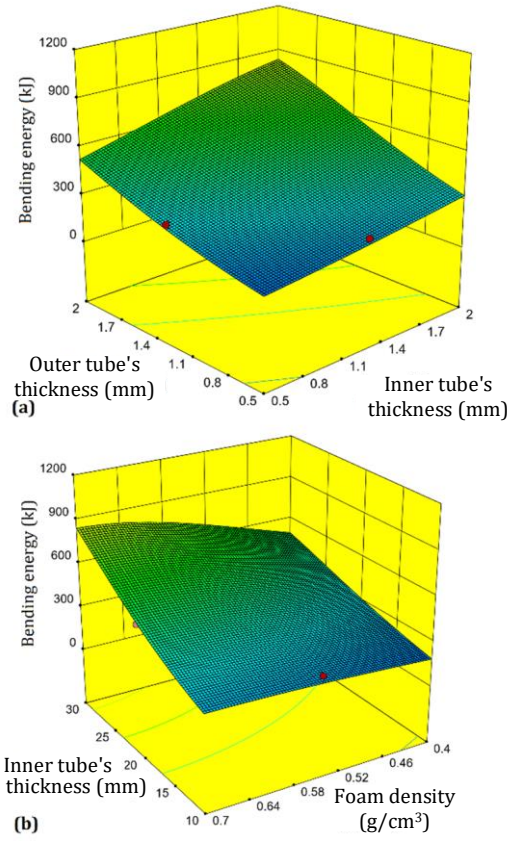

Fig. 15. Response surface plots showing the effect of (a) inner and outer tubes' thickness and (b) inner tube's diameter and foam density, on the bending energy

The optimum values of the parameters and their corresponding outputs are presented in Table 4. The values of some parameters in this table could be rounded to a more applicable value (e.g. D_i could be rounded to 30 mm). To certify the validity of the values of the optimized parameters, these values were used in a FE simulation of FFD tube bending. The force-displacement curve of this simulation and the deformed shape of the optimum FFD tube are shown in Fig. 16 and Fig. 17, respectively. Using Fig. 16, the absorbed bending energy is calculated as 678.24 kJ, which has a 4.37% difference with the bending energy obtained by optimization (, which uses the quadratic function of the bending energy). This low value of error indicates that the optimization procedure has acceptable accuracy. The optimum FFD tube has a 141.4% more energy absorption capacity than the initial configuration of the FFD tube (the configuration of FFD tube in the experimental tests of three-point bending). Moreover, the maximum bending force of the optimum FFD tube is about 27.5 kN, which is so higher than the bending force of the initial FFD tube (10.1 kN). This increase in the bending force is due to the new configuration of the FFD tube.

Furthermore, the optimum FDD tube weighs 474.25 g, which is 4.63% lower than the weight of the initial configuration of the FFD tube (453.27 g). Thus, it could be concluded that the optimization procedure led to finding a lighter tube with a more energy absorption capacity (to the initial FFD tube).

Table 4. The values of the studied parameters obtained through optimization and their corresponding outputs

Parameter	Value
D_i (mm)	29.98
$D_o - D_i$ (mm)	30.28
t_i (mm)	0.50
t_o (mm)	1.99
ρ_{foam} (g/cm³)	0.69
FFD tube weight (g)	470.05
Absorbed bending energy (kJ)	707.08

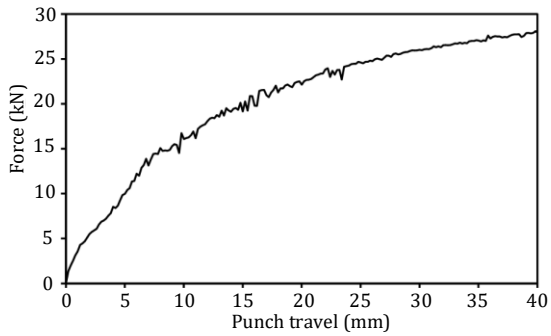

Fig. 16. Force-displacement curve of the optimized FFD tube in three-point bending

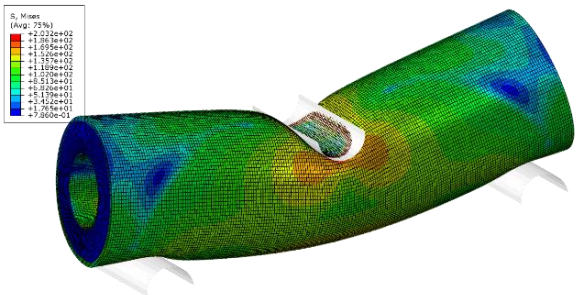

Fig. 17. Deformed shape and distribution of Mises stresses of the optimized FFD tube

5. Conclusions

In this research, the effects of D_i, D_o, t_i, t_o and ρ_{foam} parameters on the three-point bending energy and weight of FFD composite tubes are investigated using RSM. The main results could be summarized as follows:

- In the experimental tests of three-point bending tests, the maximum bending force of the FFD tube is obtained about 10 kN, which is 2.5 times larger than the sum of the maximum bending forces for the inner and outer tubes (4.13 kN). Referring to the weak flexural strength of the composite foam (bending strength of 3.8 MPa at elongation about 1%), one may conclude that FFD tube design has a very important impact on the flexural resistance of the tube.
- Comparison of FE simulation results with the experimental test results reveals that the developed FE model has good accuracy in the prediction of the bending force and energy.
- D_o-D_i and ρ_{foam} have the most and the least effects on the bending energy, respectively. While, D_o-D_i and t_i have the most and the least effects on the FFD tube's weight, respectively.
- The optimum values of D_i, D_o, t_i, t_o and ρ_{foam} are derived as (about) 30 mm, 60 mm, 2 mm, 2 mm, and 0.7 g/cm^3, respectively.
- Using the optimum values of the parameters, 141.4% increase in the absorbed bending energy and 4.63% decrease in the weight of FFD composite tube (to the experimented tube) have been obtained.

Nomenclature

σ (MPa)	Real stress
$\bar{\varepsilon}_p$	Real plastic strain
ρ_{Al} (g/cm^3)	Density of aluminum tubes
ρ_{foam} (g/cm^3)	Density of the composite foam
D_i (mm)	Inner tube's diameter
D_o (mm)	Outer tube's diameter
t_i (mm)	Inner tube's thickness
t_o (mm)	Outer tube's thickness
M (g)	FFD tube mass
L (mm)	Tube length

References

[1] Mirfendereski, L., Salimi, M. & Ziaei-Rad, S. 2008. Parametric study and numerical analysis of empty and foam-filled thin-walled tubes under static and dynamic loadings. *International Journal of Mechanical Sciences,* 50**,** 1042-1057.

[2] Najibi, A., Ghazifard, P. & Alizadeh, P. 2020. Numerical crashworthiness analysis of a novel functionally graded foam-filled tube. *Journal of Sandwich Structures & Materials***,** 1099636219900334.

[3] Li, Z., Rakheja, S. & Shangguan, W.-B. 2019. Study on crushing behaviors of foam-filled thin-walled square tubes with different types and number of initiators under multiple angle loads. *Thin-Walled Structures,* 145**,** 106376.

[4] Djamaluddin, F., Abdullah, S., Ariffin, A.K., et al. 2019. Optimisation and validation of full and half foam filled double circular tube under multiple load cases. *International Journal of Crashworthiness,* 24**,** 389-398.

[5] Santosa, S., Banhart, J. & Wierzbicki, T. 2001. Experimental and numerical analyses of bending of foam-filled sections. *Acta Mechanica,* 148**,** 199-213.

[6] Santosa, S. & Wierzbicki, T. 1999. Effect of an ultralight metal filler on the bending collapse behavior of thin-walled prismatic columns. *International Journal of Mechanical Sciences,* 41**,** 995-1019.

[7] Kim, A.K., Cheon, S.S., Hasan, M.A., et al. Bending behavior of thin-walled cylindrical tube filled with aluminum alloy foam. Key Engineering Materials, 2004. Trans Tech Publ, 46-51.

[8] Hanssen, A.G., Reyes, A.G.R., Hopperstad, O.S., et al. 2005. Design and finite element simulations of aluminium foam-filled thin-walled tubes.

[9] Guo, L., Yu, J. & Li, Z. 2010. Experimental studies on the quasi-static bending behavior of double square tubes filled with aluminum foam. *Acta mechanica,* 213**,** 349-358.

[10] Guo, L. & Yu, J. 2011. Bending behavior of aluminum foam-filled double cylindrical tubes. *Acta mechanica,* 222**,** 233-244.

[11] Shojaeifard, M.H., Zarei, H.R., Talebitooti, R., et al. 2012. Bending Behavior of Empty and Foam-Filled Aluminum Tubes with Different Cross-Sections. *Acta Mechanica Solida Sinica,* 25**,** 616-626.

[12] Duarte, I., Vesenjak, M., Krstulović-Opara, L., et al. 2015. Manufacturing and bending behaviour of in situ foam-filled aluminium alloy tubes. *Materials & Design,* 66, Part B**,** 532-544.

[13] Vesenjak, M., Duarte, I., Baumeister, J., et al. 2020. Bending performance evaluation of aluminium alloy tubes filled with different cellular metal cores. *Composite Structures,* 234**,** 111748.

[14] Golestanipour, M., Mashhadi, H.A., Abravi, M., et al. 2011. Manufacturing of Al/SiCp composite foams using calcium carbonate as foaming agent. *Materials Science and Technology,* 27**,** 923-927.

[15] (Din), D.I.F.N.E.V. 2008. Testing of metallic materials - Compression test of metallic cellular materials. Berlin.
[16] Astm 2000. E8M Standard Test Methods for Tension Testing of Metallic Materials.
[17] Anderson, T.A. 2005. An investigation of SDOF models for large mass impact on sandwich composites. *Composites Part B: Engineering,* 36**,** 135-142.
[18] Icardi, U. & Ferrero, L. 2009. Impact analysis of sandwich composites based on a refined plate element with strain energy updating. *Composite Structures,* 89**,** 35-51.
[19] Montgomery, D.C. 2017. *Design and analysis of experiments*, John wiley & sons.